Comparison of Biological Shapes Using Extracted Edges Analyzed with Polynomial Hermite Interpolation

Donatella Giuliani
Faculty of Agriculture, University "Politecnica delle Marche"
Via Brecce Bianche, Ancona 60131, Italy
E-mail: giulianidonatella@libero.it

Abstract

The aim of this work is the analysis of biological bi-dimensional structures in order to study their shapes during the growing process. At first we have proceeded to extraction of deformable contours of biological forms using as external forces, the generalized gradient vector flow, GGVF (Xu C. Prince I.J.,1998b). In this study, by evaluating the map of divergence associated with the GGVF field we automatically generate the initial contour using the level curves of a divergence map, therefore we obtain the final curve with a great accuracy. Finally, the study of the extracted edges was achieved by polynomial piecewise Hermite interpolation, in order to carry out a comparative analysis of morphology.

Keywords: Active contour, Spline interpolation, Shape analysis, Biological shape, Biological growth

1. Introduction

In this work biological structures at different stages of development were considered (Fig. 1), in order to analyze the form, highlight the main morphological features and study the underlined characteristics of the growing process. The organic growth takes place on a surface or along an edge, named *growth surface* or *growth curve*, respectively (Skalak R., 1982, 1996). Carefully examining a biological surface we can identify a set of curves that suggest how the process of growth has occurred. Usually the biological bodies have complex and highly variable shapes. What you can analyze is the resulting final shape and the structure of fibers with the associated most significant points, the landmarks, which remain to testify the modality of development.

2. Edge extraction

For each structure, which has been considered in our biological application, the edges are extracted by a deformable contour procedure.

Deformable geometric contour models are curves or surfaces defined within a 2D or 3D image, moving under the action of internal forces derived from the model itself and external forces coming from the image data.

Deformable models are widely used in many image analysis applications, including edge detection, shape analysis, segmentation, motion tracking.

Mathematically, in the two-dimensional case, deformable models are elastic curves defined within a given image $I(x, y)$. They are subjected to variations and modifications under the action of internal and external forces, until the resulting curve conforms to the final contours of the object that you want to extract.

Given an image $I : D \subset R^2 \to C$, at each point $(x, y) \in D$ is associated a colour in the colour space C. We suppose that a geometric contour of parametric equations $\vec{x}(s) = (x(s), y(s))$, $s \in [0,1]$ is embedded in it. The final shape of the contour to be extracted will be such as to minimize the energy associated with it, expressed by the functional:

$$E(\vec{x}) = E_{Int}(\vec{x}) + E_{Ext}(\vec{x}) = \int [\mathrm{E}_{Int}(\vec{x}(s)) + \mathrm{E}_{Ext}(\vec{x}(s))] ds \qquad (1)$$

The first term $E_{Int}(\vec{x})$ is the *internal energy* that expresses a priori knowledge of the model and relates to the degree of flexibility of the active contour, resulting from material properties such as elasticity and rigidity:

$$E_{Int}(\vec{x}(s)) = \int \frac{1}{2}\left[\alpha(s)\cdot\left|\frac{d\vec{x}}{ds}\right|^2 + \beta(s)\cdot\left|\frac{d^2\vec{x}}{ds^2}\right|^2\right]ds \qquad (2)$$

In equation (2) the term $\alpha(s)$ controls the tension of the contour, while $\beta(s)$ regularises rigidity. By increasing the intensity of $\alpha(s)$, a non-negative function of the parameter s, the tension of the curve increases, so that the result is a reduction of anomalies such as knots, loops or waves. On the other way an increasing of $\beta(s)$ produces a more flexible contour.

The second term $E_{Ext}(\vec{x}(s))$ represents the *external energy* that supports the curve a potential energy function $P(\vec{x}(s))$, which derives from the image $I(x, y)$. Its local minima correspond to the edges of the features to be extracted:

$$E_{Ext}(\vec{x}(s)) = \int P(\vec{x}(s))ds$$

In the *balloon models*, the pressure forces or inflation forces are also included among the external forces. They are used to push the active contour towards the edges to be extracted even in the presence of noise (Mc Inerney et al.,1995, 2000):

$$\vec{f}_p(\vec{x}) = F(I(x, y))\cdot\vec{n}(s)$$

where $\vec{n}(s)$ is the normal versor at each point of the contour and $F(I(x, y))$ is the force intensity.

In agreement with the calculation of variations, the contour that minimizes the total energy must satisfy the equation of Euler-Lagrange:

$$-\frac{d}{ds}\left(\alpha(s)\cdot\frac{d\vec{x}}{ds}\right) + \frac{d^2}{ds^2}\left(\beta(s)\cdot\frac{d^2\vec{x}}{ds^2}\right) + \nabla P(\vec{x}(s)) - \vec{f}_p = 0 \qquad (3)$$

where ∇ is the gradient operator. The differential equation (3) expresses the equilibrium condition between internal and external forces for the deformable model:

$$\vec{f}_{Int}(\vec{x}(s)) = -\nabla P(\vec{x}(s)) + \vec{f}_p(\vec{x}(s)) = \vec{f}_{Ext}(\vec{x}(s))$$

the resulting external forces are obtained as a sum of the gradient of the potential $P(x, y)$ and of the inflation forces.

Given a grayscale image $I(x, y)$, defined as a continuous function of the variables (x, y), we can evaluate the potential energy $P(x, y)$ associated with it, by means of one of the following expressions:

$$P(x, y) = -|\nabla I(x, y)|^2 \qquad (4a)$$

$$P(x, y) = -|\nabla(G_\sigma(x, y) * I(x, y))|^2 \qquad (4b)$$

in the equation (4b) $G_\sigma(x, y) * I(x, y)$ represents the convolution of the Gaussian kernel with standard deviation σ. For the circle in the image of Fig.2, the potential energy computed by the formulas (4a) and (4b) (with σ = 2) respectively, can be compared one another.

It appears natural to see the minimization of energy as the resolution of a static problem. To build a dynamic system that evolves toward a state of equilibrium, is far more efficient in determining a local minimum of functional (1). This system can be constructed by applying the principles of Lagrangian mechanics, which lead to a dynamic deformable model able to combine geometry and movement, creating a dynamic geometrical shape that evolves over time.

A simple example of a dynamic model can be obtained by introducing a time-variable parametric equation $\vec{x}(s,t) = (x(s,t), y(s,t))$, with a density of mass $\mu(s)$ and a damping coefficient $\gamma(s)$. In this way, we obtain the equation

$$\mu(s)\frac{\partial^2\vec{x}}{\partial t^2}+\gamma(s)\frac{\partial\vec{x}}{\partial t}-\frac{\partial}{\partial s}\left(\alpha(s)\cdot\frac{\partial\vec{x}}{\partial s}\right)+\frac{\partial^2}{\partial s^2}\left(\beta(s)\cdot\frac{\partial^2\vec{x}}{\partial s^2}\right)=-\nabla P(\vec{x}(s))+\vec{f}_p \qquad (5)$$

In equation (5) the first two terms represent the inertial and damping forces. The equilibrium is reached when the internal and external forces are equal, which implies the steady state of the active contour, so that we have

$$\frac{\partial^2\vec{x}}{\partial t^2}=\frac{\partial\vec{x}}{\partial t}=0 \qquad (6)$$

When the solution $\vec{x}(s,t)$ stabilizes, we reach the result of the equation (3). Indeed, at this point, the time derivatives vanish and we have the equation (3). Neglecting the inertial term and considering dumping, elasticity and rigidity as constant functions, we obtain a simplified version of equation (5):

$$\gamma\frac{\partial\vec{x}}{\partial t}-\alpha\cdot\frac{\partial^2\vec{x}}{\partial s^2}+\beta\frac{\partial^4\vec{x}}{\partial s^4}=-\nabla P(\vec{x}) \qquad (7)$$

A solution of (7) can be found by discretizing and solving the obtained finite linear system interactively.

The numerical solution of equation (7), can thus be reduced to the differential dynamic equation:

$$\begin{cases}\gamma(s)\dfrac{\partial\vec{x}(s,t)}{\partial t}=\alpha(s)\cdot\dfrac{\partial^2\vec{x}(s,t)}{\partial s^2}-\beta(s)\dfrac{\partial^4\vec{x}(s,t)}{\partial s^4}+\vec{F}_{Ext}(\vec{x})\\ \vec{x}(s,0)=\vec{x}_0(s)\end{cases}$$

where $\vec{F}_{Ext}(\vec{x})$ is the external force field, and $\vec{x}_0(s)$ is the initial contour. Hence the coordinates of the deformable model are independent, for sake of simplicity we refer to a single coordinate. Approximating the derivatives with finite differences and assuming the damping coefficient $\gamma(s)$ equal to one, the component of the discrete solution $\vec{x}_i=(x(ih),y(ih))$, must satisfied the equation:

$$\frac{x_i^t-x_i^{t-\Delta t}}{\Delta t}=\alpha_{i+1}\cdot\left(x_{i+1}^t-x_i^t\right)-\alpha_i\cdot\left(x_i^t-x_{i-1}^t\right)-$$
$$-\left[\beta_{i-1}\cdot\left(x_{i-2}^t-2x_{i-1}^t+x_i^t\right)-2\beta_i\cdot\left(x_{i-1}^t-2x_i^t+x_{i+1}^t\right)+\beta_{i+1}\cdot\left(x_i^t-2x_{i+1}^t+x_{i+2}^t\right)\right]+F_{Ext}\left(x_i^{t-\Delta t}\right) \qquad (8)$$

that may be written in matrix form as:

$$\frac{x^t-x^{t-\Delta t}}{\Delta t}=A\cdot x^t+F_{Ext}\left(x^{t-\Delta t}\right) \qquad (9)$$

where A is a diagonal band matrix. The equation (9) may be resolved with an iterative procedure, using the formula (11) shown below:

$$(I-\Delta t\cdot A)\cdot x^t=x^{t-\Delta t}+\Delta t\cdot F_{Ext}\left(x^{t-\Delta t}\right) \qquad (10)$$

$$x^t=(I-\Delta t\cdot A)^{-1}\cdot\left(x^{t-\Delta t}+\Delta t\cdot F_{Ext}\left(x^{t-\Delta t}\right)\right) \qquad (11)$$

We wish to outline that the solution of the differential equation associated with deformable model takes the form (11), whatever the applied external force field is.

3. Generalized Gradient Vector Flow: Initialization Problem

In this study of growing biological structures we have realized edge extraction of deformable contours using a different class of external forces, called Generalized Gradient Vector Flow, GGVF (Xu C., Prince I.J.,1997,1998b). In this case the force field used, or GGVF field, is obtained by solving differential equations which deriving from a diffusion problem, which propagate the force field gradient evaluated from the image. The GGVF force field differs from those previously treated, since the external forces are not expressed as a negative gradient of a potential function.

In the GGVF contour generation, a static vectorial field formed by two independent components can be used: the irrotational and the solenoidal one, with rotor and divergence null, respectively. In this approach we evaluate a static external force field $\vec{f}_{Ext}^{GGVF} = \vec{v}(x, y)$, so that the corresponding dynamic equation of the active contour will be

$$\frac{\partial \vec{x}}{\partial t} - \alpha \cdot \frac{\partial^2 \vec{x}}{\partial s^2} + \beta \frac{\partial^4 \vec{x}}{\partial s^4} = \vec{v}(\vec{x}) \qquad (12)$$

The numerical solution of equation (12) is obtained iteratively, in the same way used by other active contour models.

For the determination of the GGVF vector field, we start with the evaluation of the *edge map* $f(x,y) = \left|\nabla\left(G_\sigma(x,y) * I(x,y)\right)\right|^2$ or $f(x,y) = \left|\nabla\left(I(x,y)\right)\right|$, derived from the original image $I(x,y)$ and often normalized in order to reduce the dependence on absolute intensities.

The gradient $\nabla f(x,y)$ is a field whose vectors are directed towards the edges of the image, with norms significantly different from zero in proximity of them. On the contrary it is approximately zero in homogeneous regions, where the image intensities $I(x,y)$ are essentially constant.

The main limitations to be overcome in the generation of deformable contours are: 1) the convergence of the model towards the edges in regions with highly variable concavities, 2) the initialization problem, i.e. the excessive sensitivity to the shape and the initial position of the active contour, 3) the extension of the capture range. As we can see in the image of Fig.3, the convergence of the initial contours (in green) towards the edges leads only partially to the expected result.

Using the calculus of variations (Xu C., Prince I.J.,1997,1998a.1998b), the GGVF force field $\vec{v}(x,y)$ can be found by solving the following diffusion equation:

$$\vec{v}_t = g(|\nabla f|) \cdot \nabla^2 \vec{v} + h(|\nabla f|) \cdot (\vec{v} - \nabla f)$$

where ∇^2 is the Laplacian operator, $g(|\nabla f|)$ and $h(|\nabla f|)$ are space varying weighting functions, being dependent on the gradient of the edge map, generally not uniform. The function $g(|\nabla f|)$ will be monotonically non-increasing, since the vector field $\vec{v}(x,y)$ will be weakly variable far from the edges to be extracted where the image intensities are uniform. On the other hand, $h(|\nabla f|)$ should be monotonically non-decreasing, therefore, when $|\nabla f|$ is large, the vector field $\vec{v}(x,y)$ should have a trend nearly equal to the gradient of the edge map. In this way the GGVF model improves the efficiency of the vector force field $\vec{v}(x,y)$ to define contours with very pronounced concavities.

In this study we describe a method to generate automatically the initial curve, that could be able to adequately reconstruct the final contour. The effects due to initialization problem and the capture range extension are reduced using the *divergence map* of the force field, defined as

$$\tilde{I}(x,y) = div\left(\frac{\vec{v}(x,y)}{|\vec{v}(x,y)|}\right) \qquad (13)$$

For the image of Fig.3, it has been shown in Fig.4b. As we can see in Fig.5, the map of divergence associated with the field GGVF is strictly related to the initialization problem.

We can note in Fig.5 that active contour converges toward the final edge if the initial contour doesn't intersect the curve of highest intensities of the divergence map.

The map of divergence is characterized by a uniform gray background, black curves corresponding to the edges where the divergence is null, and a system of light curves with high intensity values. Furthermore we put in evidence (see blue arrows in Fig.6) the presence of a sort of "tails", pointing towards the most significant geometric points of the edge to be extracted, to which correspond highest curvature values.

Hence the expected result can be obtained by selecting as initial contour the level curve of the divergence map, drawn in Fig.7a. The level curves of intensity 153 may be used to define automatically the initial contour and the capture range extension. As we can see the edge is extracted correctly (Fig.7b).

4. Comparison of biological shapes with polynomial Hermite interpolation

In this section two oak leaves at different stages of development were considered (Fig.1), in order to analyze the forms and to highlight their main features. Usually organic bodies have complex and variable shapes. What we can analyze is the resulting shape, the fiber structures and the associated most significant points, *landmarks* or *principal growth points*, which remain to testify the manner of growing process.

For each structure considered in our biological application, the contour is extracted by the procedure described in the preceding paragraphs. For the leaf edge smaller the edge map used is shown in Fig.8, for the largest we must refer to Fig.11.

After the generation of the divergence map associated with the force field of GGVF, the level curves of intensity 153 were extracted. In both cases, we have used them as initial curves. The initialization curve (in blue) and the extracted edge (in red) were superimposed to the original image in Fig.10 and Fig.13, respectively for the small and large leaf.

Making a comparison of the extracted curves by means of the level curves of divergence map, shown in blue in Fig.10 and 13, we can notice a marked splitting of the two biological form edges in corresponding traits. This suggests a comparative analysis of the contours in order to be able to highlight the main morphological characteristics and to study the regularity of growth in subsequent phases. The two biological structures, in stages of development certainly different, are strongly characterized by zones with high curvature, with pronounced changes in the directions of tangent vectors to the edge. This leads to the use of piecewise interpolation with cubic Hermite splines for a comparative analysis.

The polynomial Hermite interpolation is not restricted to the points of the contour but includes the tangent directions in the extreme points, so that it is particularly suitable to the study of the edges of the leaves concerned.

A spline curve parameterization $\vec{x}(u)$ is a continuous map of a collection of intervals $u_0 < u_1 ..... < u_L$ into the Euclidian plane E^2 or the Euclidian space E^3. Each interval $u \in [u_i, u_{i+1}]$ is mapped onto a polynomial curve segment, the numbers u_i are called *knots*, and the set of all u_i is named *knot sequence*, the given points of the curve $\vec{x}(u_i)$ are called *junction points*.

We are interested in C^2 piecewise cubic spline curves, obtained by means polynomials of third degree continuously differentiable up to the second order at the junction points. The study of the growing curves is realized by polynomial piecewise interpolation. The growing edge is represented by as many spline curves as principal growth points are, each spline curve is formed by a variable number of polynomial segments as the number of interpolation points are.

The tangent vectors of the edge could mostly vary abruptly at the principal growth points. Therefore the interpolation scheme that is more suitable, is the cubic Hermite one, because it is not restricted to interpolation of data points. Indeed, for a given spline curve, we have to include the derivative data at the end points, that will be indicated with $\vec{m}_0 = \dot{\vec{x}}(u_0)$ and $\vec{m}_L = \dot{\vec{x}}(u_L)$ respectively.

Moreover, as we can see, the great importance of the use of tangent vector data at principal growth points is due to the observation that the shape of biological structures is conserved during the development, thanks to their reduced variation.

Using the piecewise cubic Hermite form, a single segment of each spline curve that maps the interval $[u_i, u_{i+1}]$ onto the curve segment between the known data points $\vec{x}_i = \vec{x}(u_i)$ and $\vec{x}_{i+1} = \vec{x}(u_{i+1})$, may be parameterized as

$$\vec{x}(u) = \vec{x}_i H_0^3\left(\frac{u-u_i}{\Delta_i}\right) + \vec{m}_i \cdot \Delta_i H_1^3\left(\frac{u-u_i}{\Delta_i}\right) + \vec{m}_{i+1} \cdot \Delta_i H_2^3\left(\frac{u-u_i}{\Delta_i}\right) + \vec{x}_{i+1} H_3^3\left(\frac{u-u_i}{\Delta_i}\right) \quad (14)$$

with $u \in [u_i, u_{i+1}], \Delta_i = u_{i+1} - u_i$, where $H_j^3(u)$ are cubic Hermite polynomials.

In the formula (14) $\vec{x}_i$ represents the known data points, whereas $\vec{m}_i = \dot{\vec{x}}(u_i)$, $i = 1,..L-1$ are the unknown tangent vector at $\vec{x}_i$, if we required that the interpolant has to be C^2 at any junction points the following relation must be satisfied:

$$\ddot{\vec{x}}_-(u_i) = \ddot{\vec{x}}_+(u_i) \qquad (15)$$

where $\vec{x}_-(u)$ and $\vec{x}_+(u)$ represent the polynomial curve segments mapped from the parameter intervals $u \in [u_{i-1}, u_i]$ and $u \in [u_i, u_{i+1}]$ respectively and explicitly expressed by:

$$\vec{x}_-(u) = \vec{x}_{i-1} H_0^3\left(\frac{u-u_{i-1}}{\Delta_{i-1}}\right) + \vec{m}_{i-1}\Delta_{i-1} H_1^3\left(\frac{u-u_{i-1}}{\Delta_{i-1}}\right) + \vec{m}_i \Delta_{i-1} H_2^3\left(\frac{u-u_{i-1}}{\Delta_{i-1}}\right) + \vec{x}_i H_3^3\left(\frac{u-u_{i-1}}{\Delta_{i-1}}\right) \qquad (16a)$$

$$\vec{x}_+(u) = \vec{x}_i H_0^3\left(\frac{u-u_i}{\Delta_i}\right) + \vec{m}_i \Delta_i H_1^3\left(\frac{u-u_i}{\Delta_i}\right) + \vec{m}_{i+1} \Delta_i H_2^3\left(\frac{u-u_i}{\Delta_i}\right) + \vec{x}_{i+1} H_3^3\left(\frac{u-u_i}{\Delta_i}\right) \qquad (16b)$$

the polynomial curve segments $\vec{x}_-(u)$ and $\vec{x}_+(u)$ are shown in Fig.14. The evaluation of the second derivatives $\ddot{\vec{x}}_-(u)$ and $\ddot{\vec{x}}_+(u)$ give us

$$\begin{aligned}\ddot{\vec{x}}_-(u_i) &= \frac{\vec{x}_{i-1}}{\Delta_{i-1}^2}\ddot{H}_0^3(1) + \frac{\vec{m}_{i-1}}{\Delta_{i-1}}\cdot\ddot{H}_1^3(1) + \frac{\vec{m}_i}{\Delta_{i-1}}\cdot\ddot{H}_2^3(1) + \frac{\vec{x}_i}{\Delta_{i-1}^2}\ddot{H}_3^3(1) \\ &= 6\cdot\frac{\vec{x}_{i-1}}{\Delta_{i-1}^2} + 2\cdot\frac{\vec{m}_{i-1}}{\Delta_{i-1}} + 4\cdot\frac{\vec{m}_i}{\Delta_{i-1}} - 6\cdot\frac{\vec{x}_i}{\Delta_{i-1}^2} \qquad (17a)\end{aligned}$$

$$\begin{aligned}\ddot{\vec{x}}_+(u_i) &= \frac{\vec{x}_i}{\Delta_i^2}\ddot{H}_0^3(0) + \frac{\vec{m}_i}{\Delta_i}\cdot\ddot{H}_1^3(0) + \frac{\vec{m}_{i+1}}{\Delta_i}\cdot\ddot{H}_2^3(0) + \frac{\vec{x}_{i+1}}{\Delta_i^2}\ddot{H}_3^3(0) \\ &= -6\cdot\frac{\vec{x}_i}{\Delta_i^2} - 4\cdot\frac{\vec{m}_i}{\Delta_i} - 2\cdot\frac{\vec{m}_{i+1}}{\Delta_i} + 6\cdot\frac{\vec{x}_{i+1}}{\Delta_i^2} \qquad (17b)\end{aligned}$$

so by condition (15), after short calculations, we could obtain the equations (Farin G.,1990,2000):

$$\vec{m}_{i+1}\Delta_{i-1} + \vec{m}_{i-1}\Delta_i + 2\cdot(\Delta_i + \Delta_{i-1})\cdot\vec{m}_i = 3\left[\frac{\Delta_i\cdot(\vec{x}_i - \vec{x}_{i-1})}{\Delta_{i-1}} + \frac{\Delta_{i-1}\cdot(\vec{x}_{i+1} - \vec{x}_i)}{\Delta_i}\right] \qquad i = 1,...L-1 \quad (18)$$

This linear system has the tangent vectors $\vec{m}_i$ $i = 1,...L-1$ as unknowns. Its solution will give us the final interpolating curve, using the data points $\vec{x}_i, i = 0,...L$ and the tangent vectors $\vec{m}_0, \vec{m}_L$ at the end points.

Furthermore, the resolution of the linear system (18) give us, after a normalization, so many values of *tangent vectors*, as the data points are.

By resolving it (18), we could directly evaluate the angles formed by the tangent vectors $\vec{m}_i = \left(m_x\big|_i, m_y\big|_i\right)$ with the horizontal axis, by means

$$\theta(u_i) = \arctan\left(\frac{m_x\big|_i}{m_y\big|_i}\right) \qquad i = 1, L-1$$

Thereafter, by observing the expressions $(17a)$ or $(17b)$ we could immediately evaluate the signed curvature at the inner points of each piece, with the following formula:

$$k(u_i)=\frac{\det\left|\dot{\vec{x}}_i(u_i),\quad \ddot{\vec{x}}_i(u_i)\right|}{\left|\dot{\vec{x}}_i(u_i)\right|^3}=\frac{\det\left|\vec{m}_i\,,\quad 6\cdot\frac{\vec{x}_{i-1}}{\Delta_{i-1}^2}+2\cdot\frac{\vec{m}_{i-1}}{\Delta_{i-1}}+4\cdot\frac{\vec{m}_i}{\Delta_{i-1}}-6\cdot\frac{\vec{x}_i}{\Delta_{i-1}^2}\right|}{\left|\vec{m}_i\right|^3}\qquad i=1,..L \quad (19)$$

As we can see in the application, the analysis of the tangent curve could define a *shape function* corresponding to each piece of the biological form, that may characterize a standard behaviour of the growing curve.

In the figures from 15a to 17b, we have graphically represented curvature $k(u)$ and angle of tangent vectors $\theta(u)$ versus a normalized curvilinear abscissa, evaluated for the two leaves corresponding sections and defined by the edge maps associated to the contours of Fig.10 and Fig.13.

For each section was assessed a polynomial curve with a best-fitting procedure, that approximates the represented data. The images are displayed in succession in order to facilitate a comparative view.

As we can see, the analogy between the interpolated curves shows a good regularity of the growth process for the analyzed biological forms.

5. Conclusions

In this paper we have presented a method for comparing bi-dimensional biological structures in different growing phases, in order to investigate the regularity of the growth process. After the extraction of edges with the active contour method GGVF, the study of the edges was achieved by polynomial piecewise Hermite interpolation, in order to carry out a comparative morphological analysis of homologous segments. We may conclude that the growing form results strongly characterized by the tangent vectors trend of corresponding traits. Therefore the analysis of the geometrical shape of biological edges may lead to the definition of standard reference forms for them.

Acknowledgements

We would like to thank Prof. Naldi Giovanni (Department of Mathematics "Federigo Enriques", University of Milan – Italy) for the helpful contribution given in this study, and the Dott.ssa Barboni Benedetta for the support in the article's revision.

References

Cohen L.D. (1991). On active contour models and baloons, *CVGIP: Imag. Under,* Vol. 53,N. 2,1991, pp. 211-218.

Farin G. (1990). *Curves and surfaces for computer aided geometric design*, Ed. Academic Press, 1990.

Farin G., Hansford D. (2000). *The essentials of CAGD*, Ed. A. K. Peters, Wellesly Mass. U.S.A.

Mc Inerney T., Terzopoulos D. (1995). A dynamic finite element surface model for segmentation and tracking in multidimensional medical images with application to cardiac 4D image analysis, *Computerized Medical Imaging and Graphics*, 19(1),pp. 69–83, 1995.

Mc Inerney T., Terzopoulos D.,T-snakes. (2000). Topology adaptive snakes, *Medical Image Analysis*, Vol. 4, 2000, pp. 73-91.

Park J.Y., Mc Inerney T.,Terzopoulos D., Myoung-Hee K. (2001). A non-self-intersecting adaptive deformable surface for complex boundary extraction from volumetric images*, Computer & Graphics 2*5, 2001, pp 421-440.

Skalak R., Dasgupta G., and Moss M. (1982). Analytical Description of Growth, *Journal Theor. Biol.*, 94, 1982, pp 555-577

Skalak R., Farrow D., and Hoger T. (1996). Kinematics of Surface Growth, *Journal Math. Biol.*,1996, pp 869-907.

Terzopoulos D., Witkin A., Kass M. (1988). Contraints on deformable models: recovering 3D shape and non rigid motion, *Artif. Intell.*, Vol. 36, N.1, 1988, pp 91-123.

Terzopoulos D.,Fleischer K. (1988). Deformable model, *The Visual Computer*, 4,pp. 306–331, 1988.

Xu C., Prince L.J. Gradient Vector Flow: a New External Force for Snakes, IEEE Proc.Conf. on *Comp. Vis. Patt. Recogn.*, CVPR'97, pp 66

Xu C., Prince L.J. (1998). Snakes, shapes, and gradient vector flow, IEEE Trans. on *Image Processing*, 7, 1998a, pp 359.

Xu C., Prince L.J. (1998). Generalized gradient vector flow external forces for active contours, *Signal Processing, an International Journal*, 71, 1998b, pp 132.

Xu C., Prince L.J. (2000). *Handbook of Medical Imaging*, Ed Isaac Bankman, Academic Press.

Figure 1. Two oak leaves at different stages of development

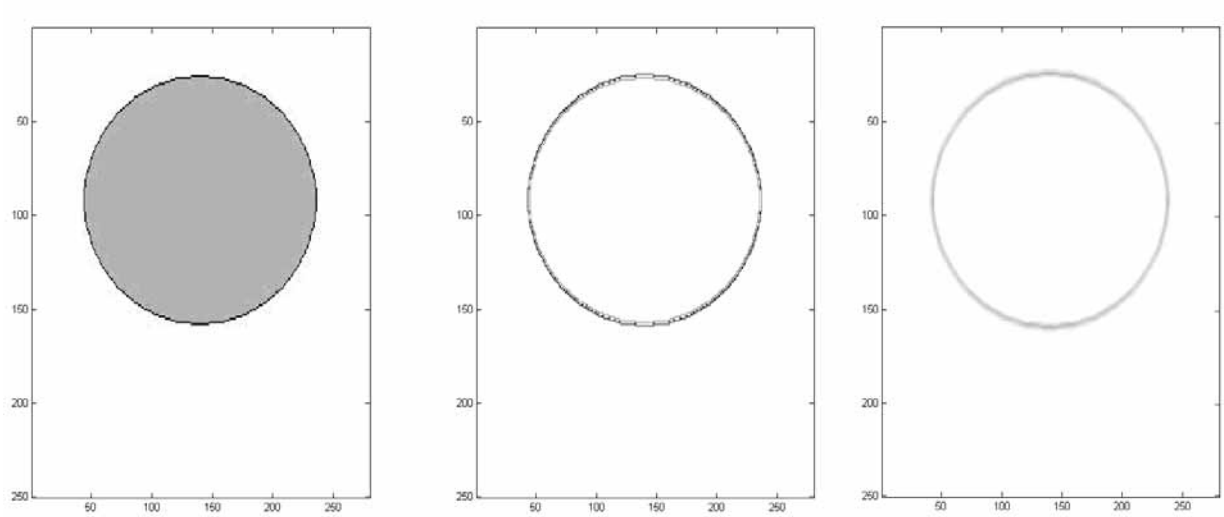

Figure 2. Image $I(x,y)$, Potential Energy: $P(x,y) = -|\nabla I(x,y)|^2$ and $P(x,y) = -|\nabla(G_\sigma(x,y) * I(x,y))|^2$

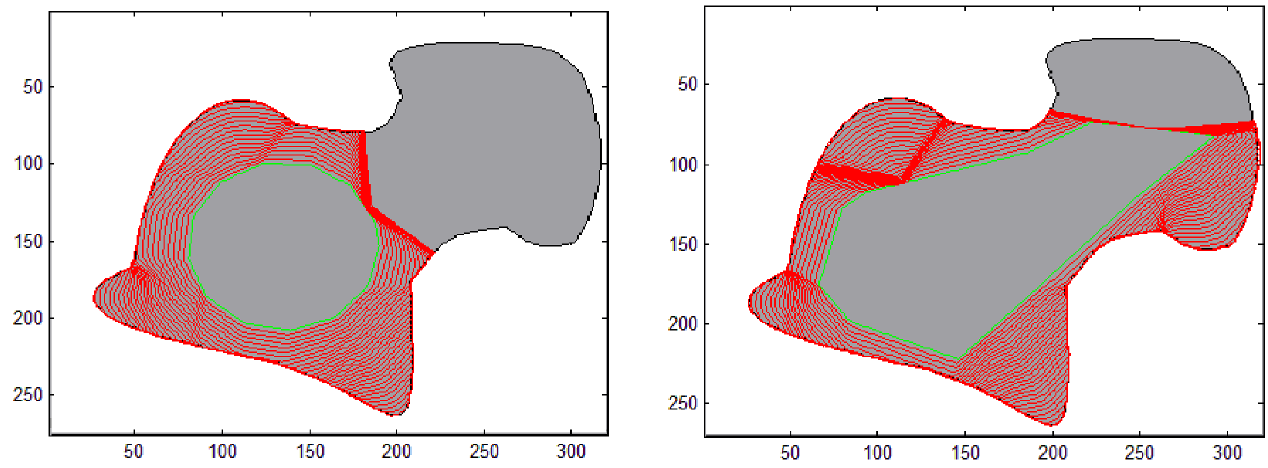

Figure 3. The initialization problem for active contour

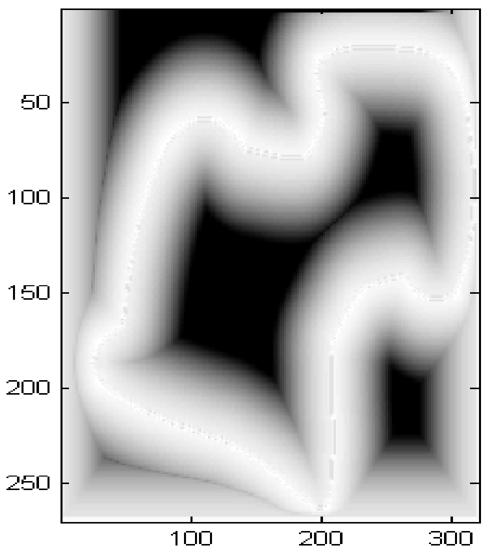

Figure 4a: $\tilde{I}(x, y) = \log|\vec{v}(x, y)|$

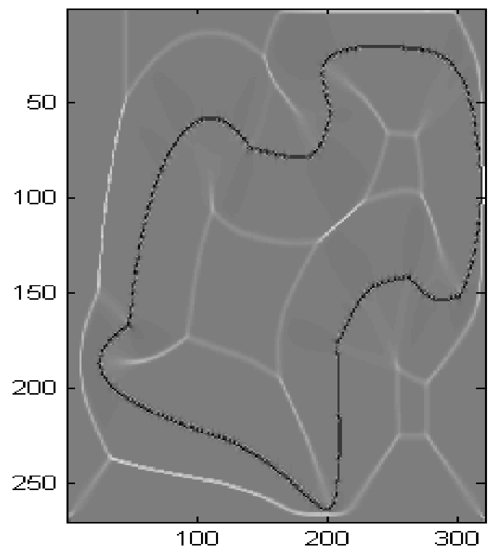

Figure 4b. $\tilde{I}(x, y) = div\left(\frac{\vec{v}}{|\vec{v}|}\right)$ GGVF Field

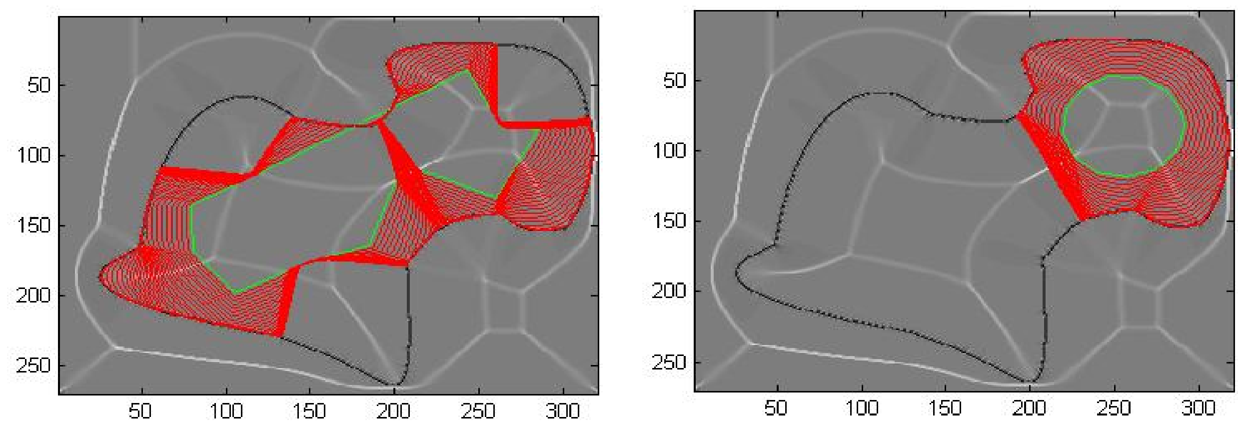

Figure 5. Initial contour of arbitrary shape and position

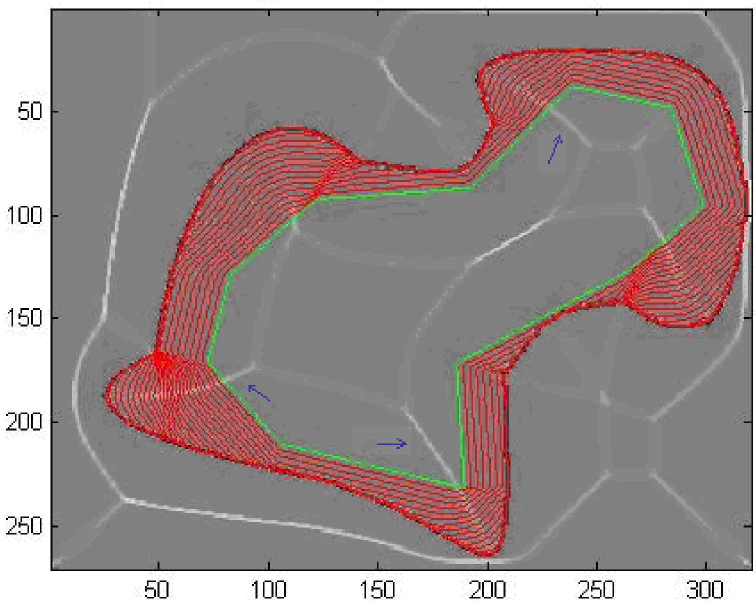

Figure 6. Initial contour selected by means the divergence map

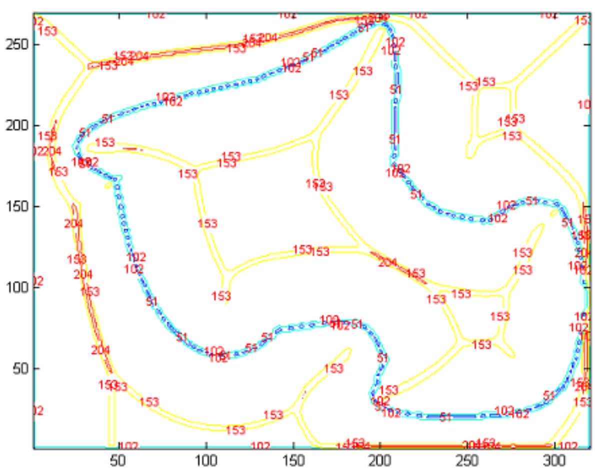

Figure 7a. Level Curves of Divergence Map

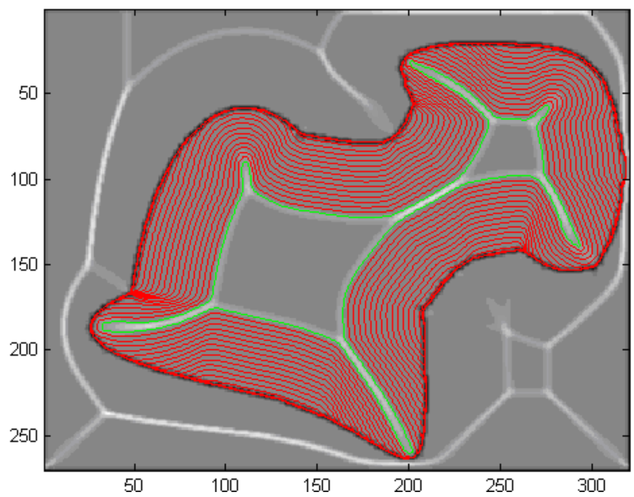

Figure 7b. Initial contour selected from Divergence Map

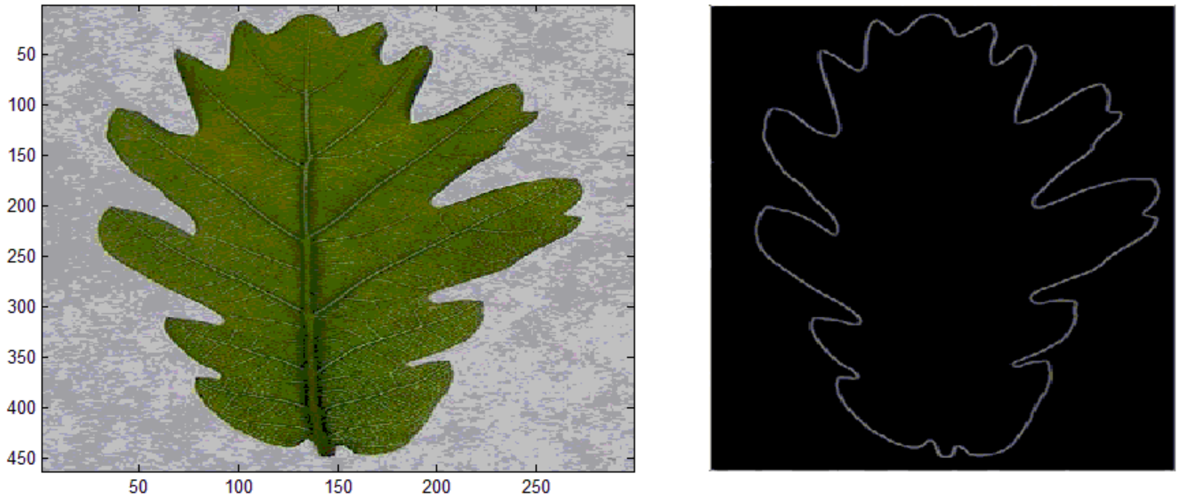

Figure 8. Small leaf and associated edge map

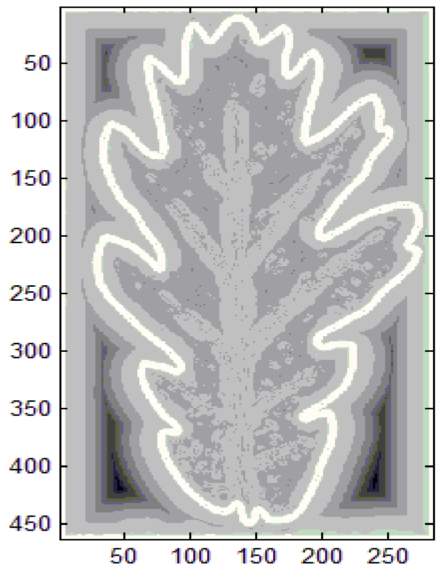

Figure 9a. $\widetilde{I}(x, y) = \log|\vec{v}(x, y)|$

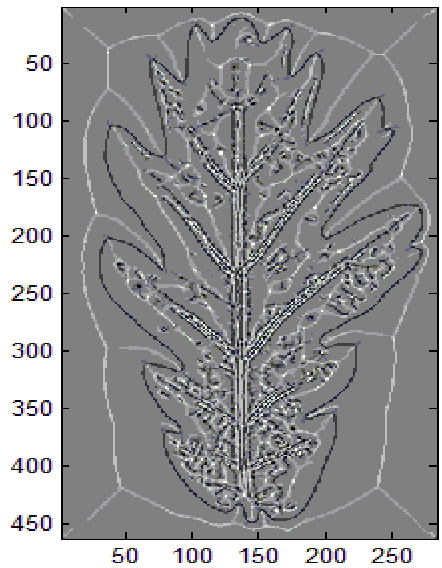

Figure 9b. $\widetilde{I}(x, y) = div\left(\frac{\vec{v}}{|\vec{v}|}\right)$

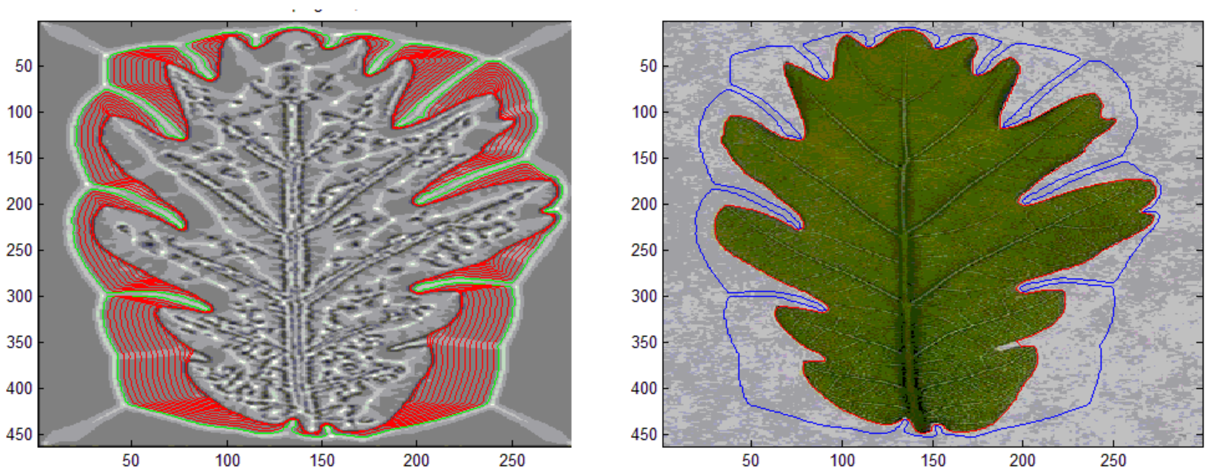

Figure 10. Extracted edge of small leaf with initial contour generated automatically

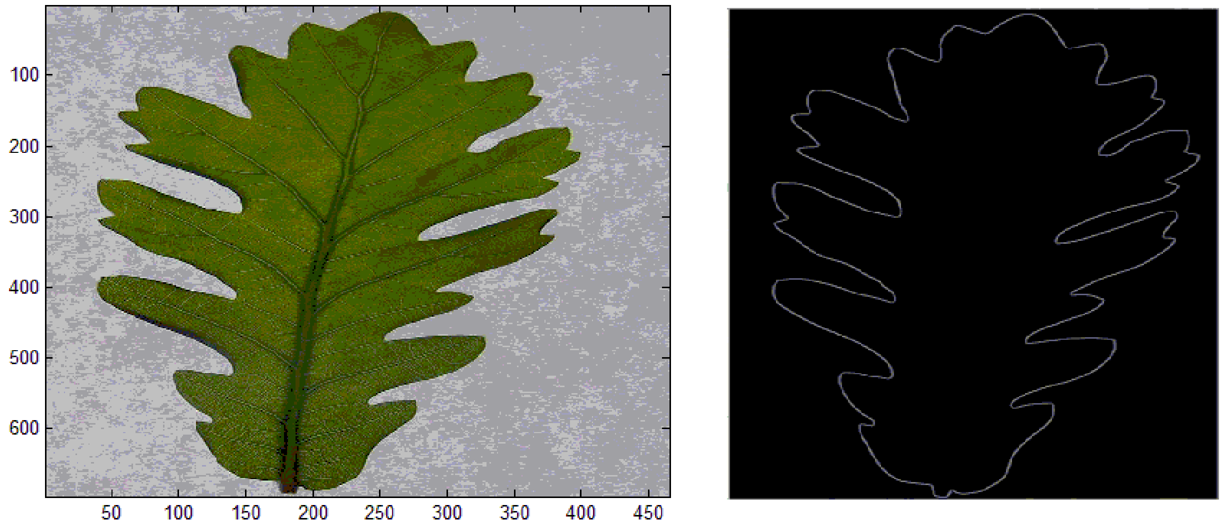

Figure 11. Large leaf and associated edge map

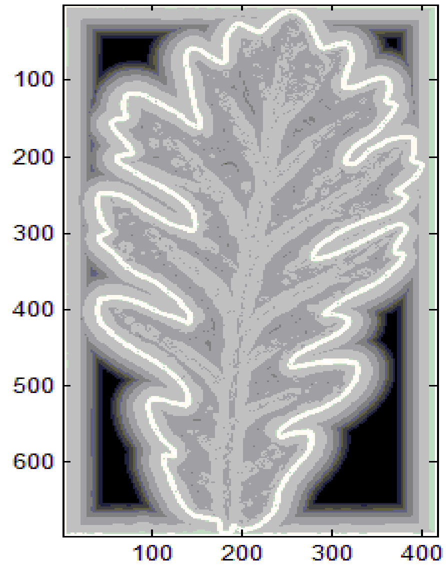

Figure 12a. $\tilde{I}(x,y)=\log|\vec{v}(x,y)|$

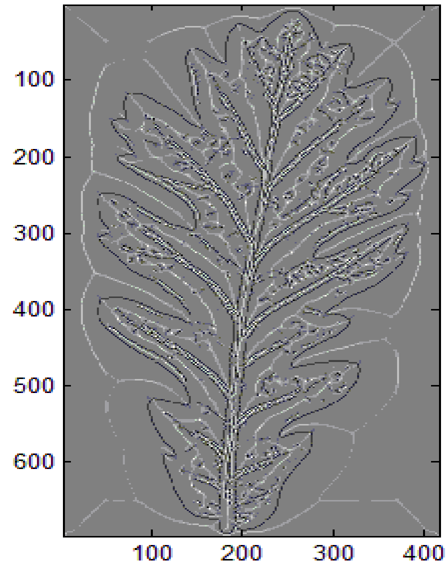

Figure 12b. $\tilde{I}(x,y)=div\left(\frac{\vec{v}}{|\vec{v}|}\right)$

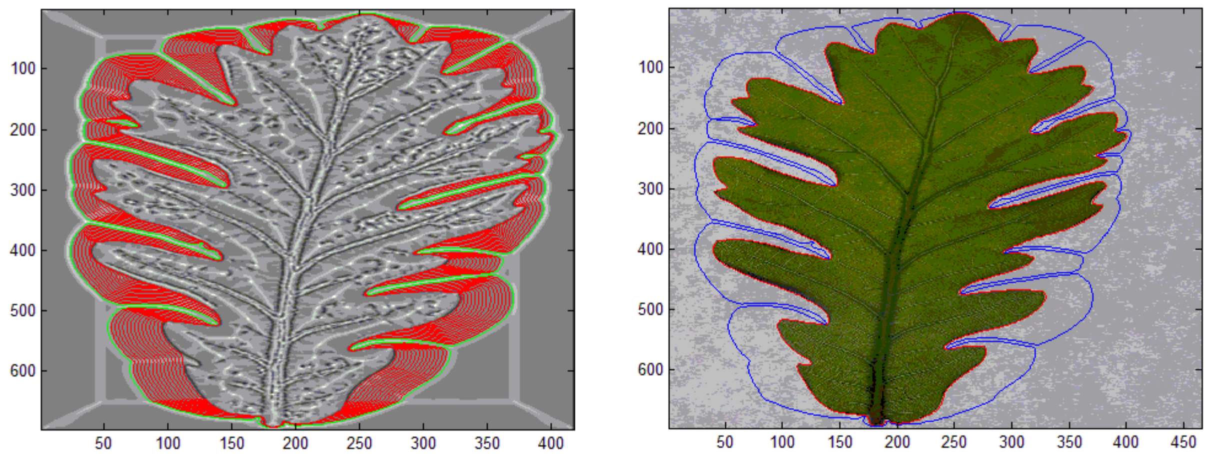

Figure 13. Extracted edge of large leaf with initial contour generated automatically

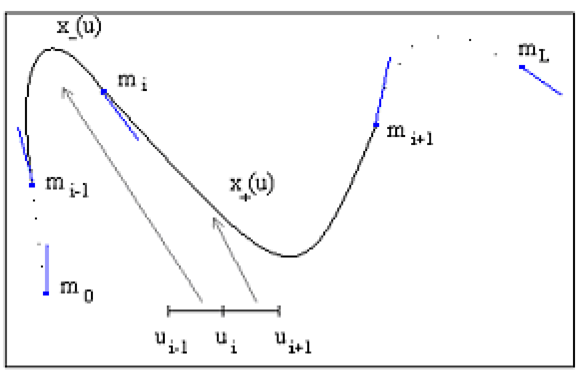

Figure 14. The polynomial curve segments $\vec{x}_{-}(u)$ and $\vec{x}_{+}(u)$

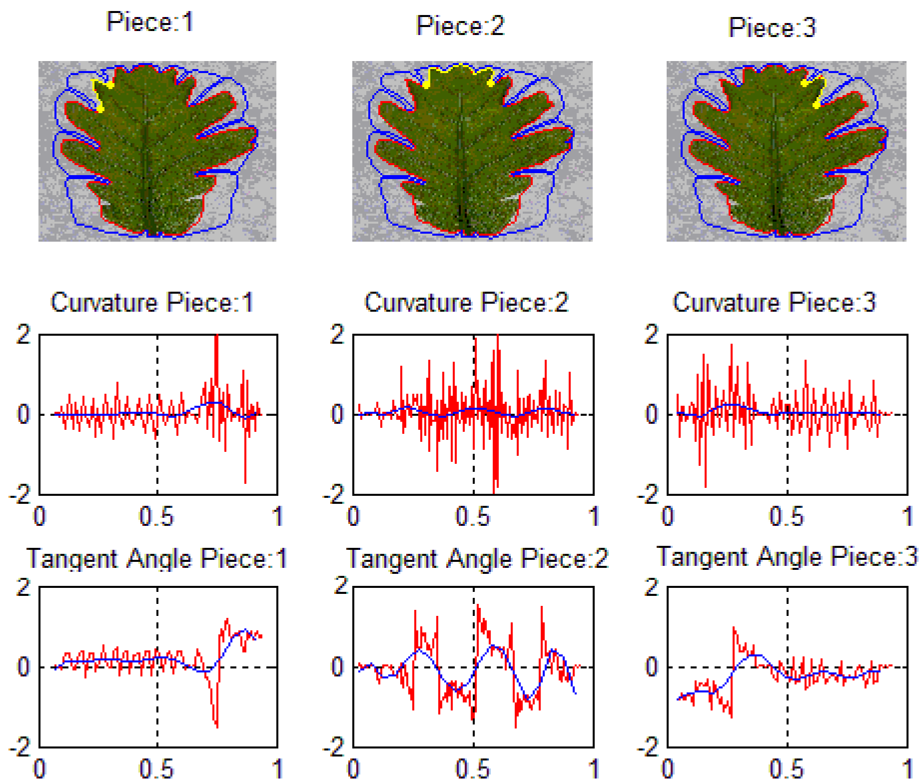

Figure 15a. Curvature $k(u)$ and angle of tangent vectors $\theta(u)$ of the small leaf

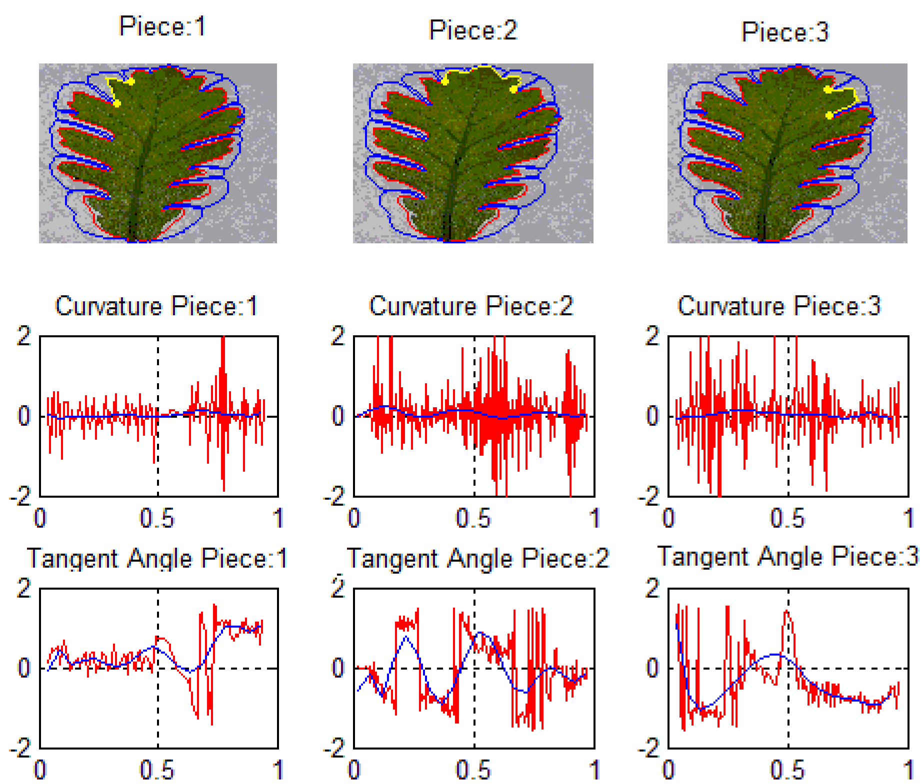

Figure 15b. Curvature $k(u)$ and angle of tangent vectors $\theta(u)$ of the large leaf

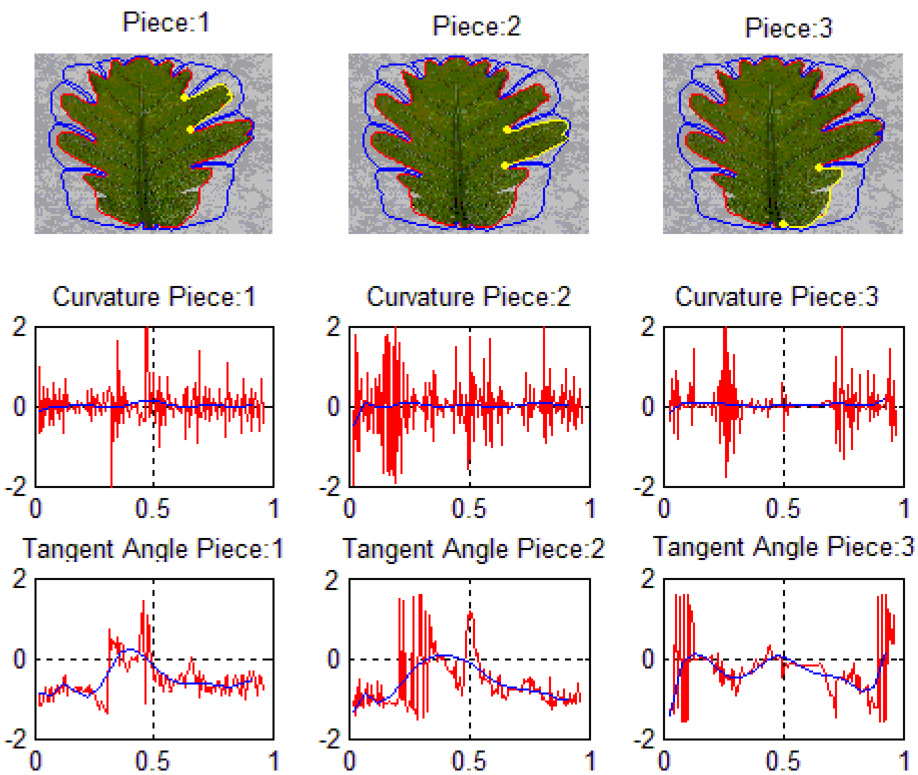

Figure 16a. Curvature $k(u)$ and angle of tangent vectors $\theta(u)$ of the small leaf

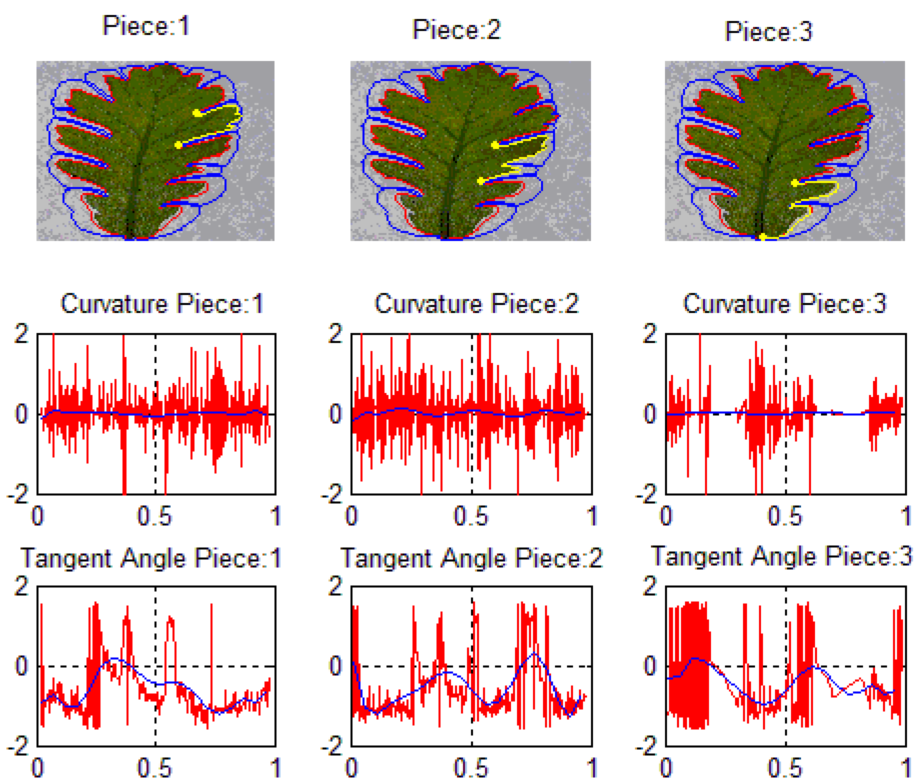

Figure 16b. Curvature $k(u)$ and angle of tangent vectors $\theta(u)$ of the large leaf

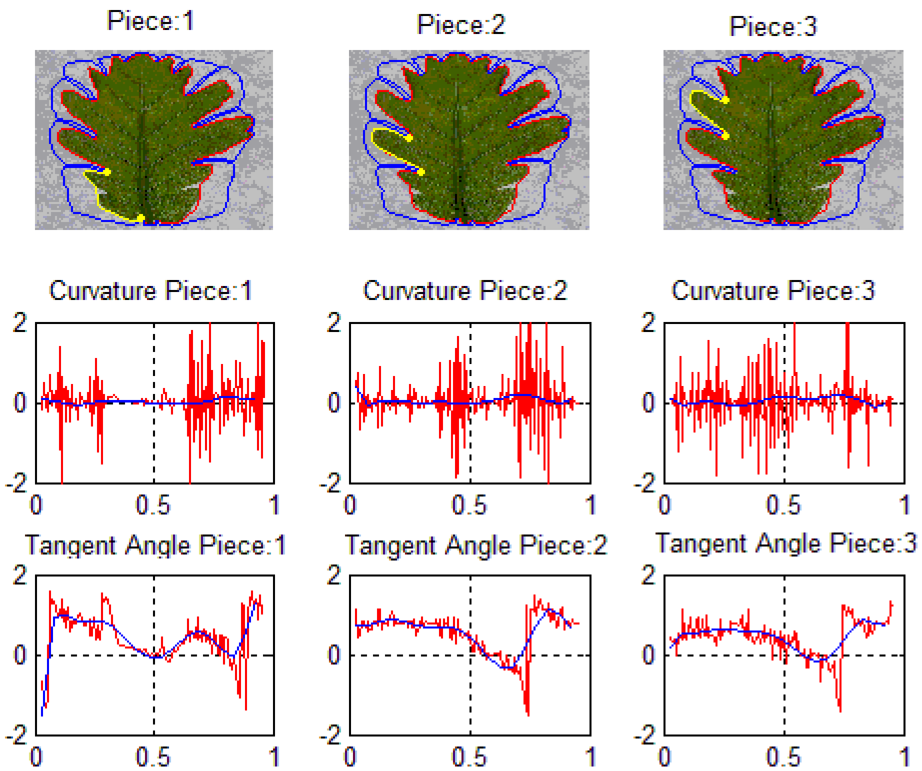

Figure 17a. Curvature $k(u)$ and angle of tangent vectors $\theta(u)$ of the small leaf

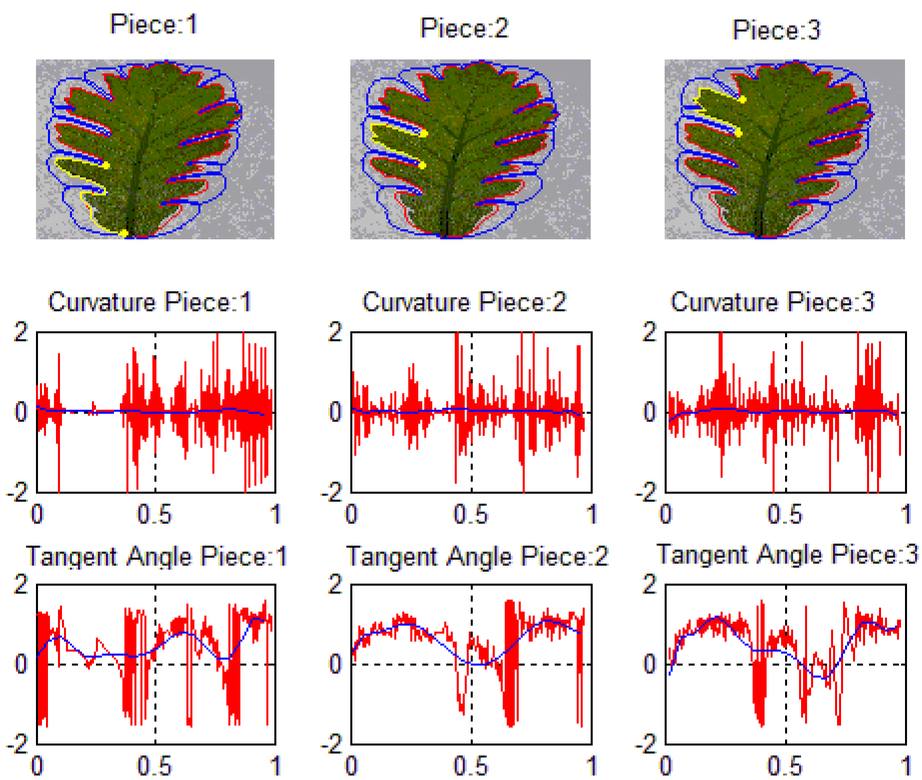

Figure 17a. Curvature $k(u)$ and angle of tangent vectors $\theta(u)$ of the large leaf